chemengineering

MDPI

Article

Nanohybrid Layered Double Hydroxides Used to Remove Several Dyes from Water

Karima Abdellaoui [1,2], Ivana Pavlovic [1] and Cristobalina Barriga [1,*]

[1] Departamento de Química Inorgánica e Ingeniería Química, Instituto Universitario de Química Fina y Nanoquímica (IUQFN), Universidad de Córdoba, Campus de Rabanales, Edificio Marie Curie, 14071 Córdoba, Spain; karimaabdellaoui18@yahoo.com (K.A.); iq2pauli@uco.es (I.P.)

[2] Laboratoire Physico Chimie des Matériaux Catalyse et Environnement, Universitè des Sciences et de la Technologie d'Oran-Mohamed Boudiaf, Oran 31000, Algeria

* Correspondence: cbarriga@uco.es

Received: 10 February 2019; Accepted: 14 April 2019; Published: 19 April 2019

Abstract: For the preparation and characterization of several layer double hydroxides (LDH) with inorganic interlayer anions (carbonate and nitrate) and nanohybrids, two organo-LDHs were studied in detail. The dodecylbenzene sulfonate (DBS) was used as an organic interlayer anion to modify the hydrophilic nature of the interlayer. The aim of the modification of the layered double hydroxides (LDH) was to change the hydrophilic character of the interlayer to hydrophobic with the purpose of improving its ability to adsorb several (anionic and cationic) dyes from water. These compounds have been used as adsorbents of amaranth (Am), diamine green B (DGB) and brilliant green (BG) dyes. Adsorption tests were conducted using variable pH values, contact times and initial dye concentrations (adsorption isotherms) to identify the optimum conditions for the intended purpose. Adsorbents and adsorption products were characterized by several physicochemical techniques. The results of the adsorption tests showed that the organo-LDH nanohybrids could be efficient adsorbents in the removal of studied dyes from water. Thus, it can be concluded that nanohybrids studied in this work might act as suitable supports in the design of adsorbents for the removal of a wide spectrum of dyes with the aim of reducing the adverse effects on water resources.

Keywords: layered double hydroxide; hydrotalcite; nanohybrid; dyes; adsorption; amaranth; diamine green B; brilliant green

1. Introduction

Organic pollutants are often detected in natural waters, and this has raised concerns regarding the protection of health and the environment [1,2]. Dyes are a complex class of organic compounds with a wide range of applications in the textile and food industries, with a large amount of dyes being wasted, reaching natural water resources. Due to their chemical structure, dyes are resistant to light, many chemicals, oxidants and heat, and they are not biodegradable, and, therefore, once released into the aquatic environment, are difficult to eliminate. If not treated appropriately, dyes may cause serious environmental problems [3] and it is very important to identify appropriate treatments for dye wastewaters [4]. Different physicochemical techniques including membrane filtration, coagulation, electrochemical methods, oxidation, adsorption and biological technology have been developed for the remediation of dye wastewaters [5–7], adsorption being one of the most suitable methods due to its efficacy and low cost [8]. There are numerous studies using different low-cost adsorbents such as sludge, rice husks, bentonite, fly ash, chitosan and some agricultural by-products to remove dye from wastewater [8–13]. Each of these adsorbents may perform well for the adsorption of a single kind of dye, but the adsorption capacity is quite variable. Therefore, the reported adsorption capacities should

be analyzed with caution since these values are dependent on the characteristics of the material and the experimental conditions [14]. Dye wastewater released from factories often contains several kinds of these contaminants (anionic, cationic, non-polar, etc.) [15] and, therefore, it is important to find a broad-spectrum adsorbent for this aim.

Layered double hydroxides (LDH), also known as hydrotalcite-like compounds, have been reported as efficient adsorbents for anionic contaminants from water [16–20]. These compounds consist of brucite-like layers which contain the hydroxides of divalent (M^{II}) and trivalent (M^{III}) metal ions and have an overall positive charge balanced by hydrated anions between layers and present a general formula $[M^{II}_{(1-x)}M^{III}_{x}(OH)_2]^{x+}(A^{n-})_{x/n}\cdot mH_2O$, where A^{n-} is the intercalated anion. LDH has a hydrophilic nature due to the strong hydration interlayer inorganic anions, but their surface properties could be changed to hydrophobic by intercalating of large organic anions into the interlayer space.

These organo-LDH with a suitable intercalated anion can provide interlayer spaces between 2 and 4 nanometers and might be considered as nanohybrids with hydrophobic characteristics in the interlayer and external surface [21–24]. In this way, the adsorption ability of these compounds for organic pollutants could be significantly improved [25–29].

In comparison with some other adsorbents of water contaminants such as clay minerals and activated carbon, LDH has some advantages: apart from being less expensive than activated carbon, they are more suitable for capturing anionic contaminants than clay minerals such as brucite which do not have any layer charge, and smectite which has negatively charged layers and thus adsorbs cationic pollutants by ion exchange. Furthermore, the LDH interlayer could be modified from hydrophilic to hydrophobic which could favour the adsorption of low polar contaminants even cationic contaminant. Thus, we chose LDH with different interlayer anions in order to study their different adsorption behaviour for anionic azo dyes Am and DGB, and cationic dye BG. These dyes have been selected for this adsorption study because they have a widespread use and thus present potential water contaminants [30].

There are different methods in the literature [18,31] that allow the synthesis of LDH materials with tailor-made physical and chemical properties appropriate in many applications. Coprecipitation, the urea method, induced hydrolysis, rehydration and reconstruction, the sol-gel technique, hydrothermal, microwave, and ultrasound treatments and anion-exchange reactions [31]. To obtain LDH with high chemical homogeneity, coprecipitation at constant pH is recommended [32] and this is the method used in this work which has also been chosen by its ease and speed in the preparation, and the previous experience in the preparation of hydrotalcite-type compounds with inorganic and organic anions in the interlayer space [16,17,26,29].

In this work, four different LDHs were prepared: two with inorganic anions, carbonate and nitrate (named MgAlCO3 and MgAlNO3, respectively) and the other two nanohybrids intercalated with dodecylbenzene sulfonate (DBS) with a different ratio Mg/Al = 3 and 2 (named Mg2AlDBS and Mg3AlDBS, respectively) with the aim to assess the removal of dyes of different natures: amaranth (Am), diamine green B (DGB) and brilliant green (BG) from water. The dyes are used not only for the coloration of textiles, plastics, paints, inks, and lacquers, but also for high-tech applications such as optical data storage, reprographics, display devices, dye-sensitized solar cells, light-emitting diodes, laser welding processes, etc. [30].

2. Results and Discussion

2.1. Characterization of the Adsorbents

The results of the elemental analysis of the adsorbents prepared are shown in Table 1 together with other characteristics. The amount of organic anion was determined from the ratio S/Al for the samples Mg2AlDBS and Mg3AlDBS. The content of S indicates that the layer charge in MgxAlDBS (x = 2 and 3) is balanced only by the organic anion. The amount of S was more than that required in order to compensate the layer charge, suggesting that the excess of DBS remained as Na salt, according

to the Na analysis (Table 1). The ratio Mg/Al = 2 and 3 was used in order to increase the charge density of the layers and consequently the content of interlayer anions as shown in Table 1.

The proposed formulae were obtained from the elemental analysis, assuming that all the positive charge is compensated by the maximum amount possible of carbonate, nitrate and dodecylbenzene sulfonate anion (DBS) for MgAlCO3, MgAlNO3 and MgxAlDBS, respectively. The amount of water was attained from thermogravimetric analysis (TGA) data and the metal content analysis. TGA curves of MgAlCO3, MgAlNO3 are reported in [19] and TGA curves of MgxAlDBS are included in Figure S1.

Table 1. Elemental analysis results and some structural data for the MgAlCO3, MgAlNO3, Mg2AlDBS and Mg3AlDBS samples.

Sample	%Al	%Mg	%S	%Na	Mg/Al	a (nm)	c (nm)	S_{BET} (m^2/g)	Formulae
MgAlCO3	10.49	19.16	-	-	2.03	0.304	2.28	78	$[Mg_{0.67}Al_{0.33}(OH)_2](CO_3)_{0.165}0.64H_2O$
MgAlNO3	9.76	17.26	-	-	1.96	0.304	2.64	10	$[Mg_{0.66}\ Al_{0.34}(OH)_2](NO_3)_{0.34}1.18H_2O$
Mg2AlDBS	3.54	6.71	6.11	1.28	2.1	0.303	9.07	7	$Mg_{0.68}Al_{0.32}(OH)_2](DBS)_{0.32}(DBSNa)_{0.13}1.02H_2O$
Mg3AlDBS	2.81	7.70	5.81	1.59	3.04	0.305	9.11	11	$Mg_{0.75}Al_{0.25}(OH)_2](DBS)_{0.25}(DBSNa)_{0.165}0.74H_2O$

The powder X-ray diffraction (PXRD) patterns of the prepared samples were analyzed with Diffract EVA 3.1 Program and reported in Figure 1, and show a typical pattern of hydrotalcite-like compounds with a series of strong basal reflections indexed, assuming a rhombohedral structure, as (*003*), (*006*), etc. These basal reflections correspond to the successive orders of the basal (interlayer) spacing c′. The interlayer spacing c′ is estimated by the formula $(d_{003} + 2d_{006} + \ldots + nd_{00(3n)})/n$. The cell parameter c is a multiple of the interlayer spacing c′, depending on the layer stacking sequence, c = 3c′ for rhombohedral structure (3R). The higher-order reflections (n = 3) are more pronounced in organic LDH compounds. Among the various non basal reflections (hkl, neither h nor k being zero), the (*110*) reflection gives a direct measure of a ($a = 2d_{110}$). It should be noted, however, that the adjacent (*113*) peak often overlaps the (*110*) one [31].

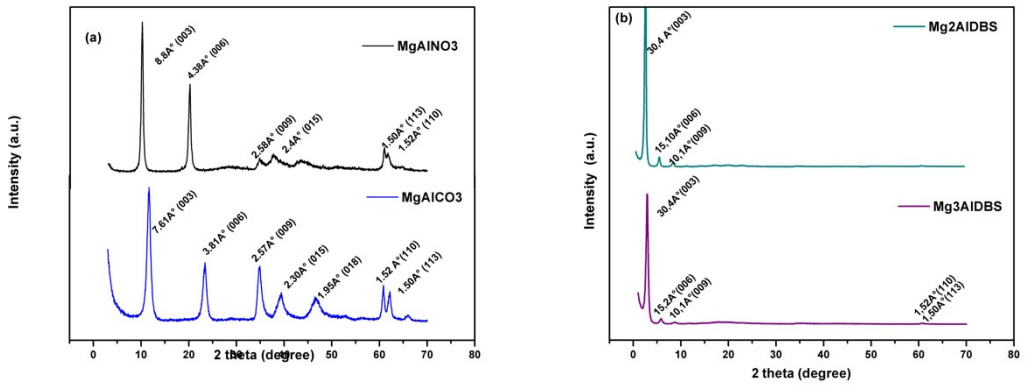

Figure 1. PXRD pattern of the synthetized adsorbents: (**a**) MgAlCO3 and MgAlNO3 LDH samples, (**b**) Mg2AlDBS and Mg3AlDBS nanohybrids samples.

The corresponding values of the a and c parameters for the adsorbents are also included in Table 1. As expected, the positions of the basal reflections of all the prepared organo-LDH hybrids are shifted to smaller 2θ reflection angles regarding inorganic hydrotalcite, which reveals expansion in the interlayer distances. Moreover, several harmonics are also observed indicating a well-ordered structure. The range of interlayer distances from a hydrotalcite with DBS in its interlayer can vary between 2.6 and 3.0 nm, depending on the orientation of dodecylbenzenesulfonate anions and on the drying method [21]. When the alkyl chains are oriented in the perpendicular position with benzene rings tilted toward the layer, and water molecules remain adsorbed between the methyl end group and the hydroxyl layer, the spacing is about 3.0 nm [32–34].

The Fourier Transform Infrared spectra (FT-IR) of the samples are included in Figure 2 and were characteristic of LDH compounds [18]. The most representative features are: a broad band

around 3500 cm^{-1} corresponding to the hydroxyl groups vibrations, a band at 1632 cm^{-1} due to the bending mode of water molecules and a band at 1380 cm^{-1} due to the vibration of carbonate and/or nitrate anions. In the FT-IR spectra of the nanohybrids (Figure 2b) are also present dodecylbenzene sulfonate features: bands at 2800–3000 cm^{-1} and 1467 cm^{-1} due to C–H stretching and deformation vibration modes, respectively, and several bands in the region 1270–800 cm^{-1} due to the sulfonate group vibrations.

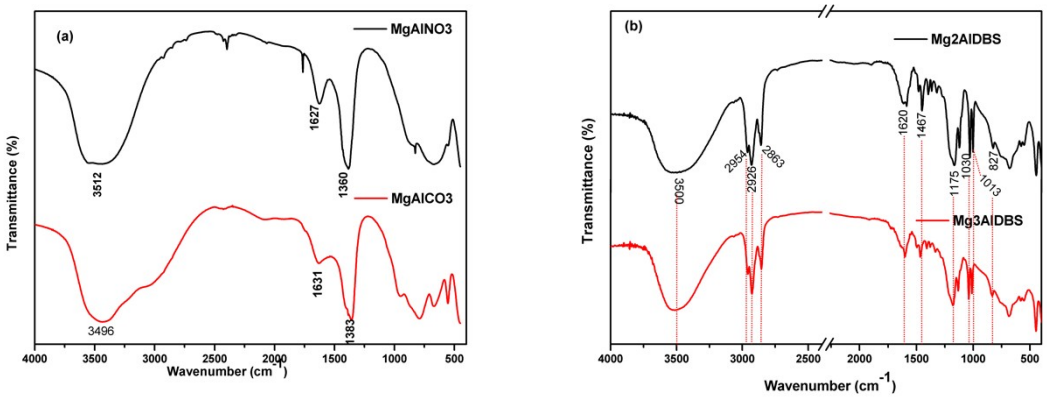

Figure 2. FT-IR spectra of the synthetized adsorbents: (**a**) MgAlCO3 and MgAlNO3 LDH samples; (**b**) Mg2AlDBS and Mg3AlDBS nanohybrids' samples.

The SEM images, included in Figure 3, showed that the MgAlCO3 sample has a sand-rose morphology (Figure 3a), whereas the particles of Mg2AlDBS (Figure 3b) are aggregated probably via hydrophobic interactions, and less defined particle surfaces are observed. This suggests that an excess of DBS could coat the outer surfaces [35,36].

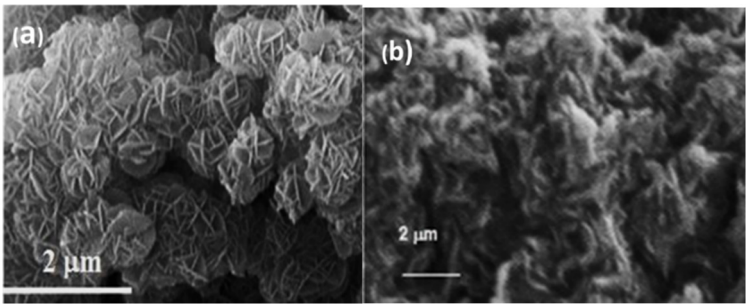

Figure 3. SEM photographs of the adsorbents: (**a**) MgAlCO3 and (**b**) Mg2AlDBS.

The curves obtained from N_2 adsorption and desorption analysis are shown in Figure S2 and correspond to type IV according to the IUPAC classification and are therefore characteristic of these mesoporous materials [37]. A notable characteristic of the type IV isotherm is the presence of the hysteresis loop which is associated with the condensation of N_2 in the pores. The values of BET surface are included in Table 1 and are quite low, as is characteristic of LDH compounds [38].

The zeta potential values of the MgAlCO3, MgAlNO3 and MgxAlDBS samples were measured in a KCl solution (0.01 M) at pH between 2 and 12, and the data are included in Figure S3. The results suggested a positive charge density on the inorganic LDH surfaces. When the anionic surfactant was intercalated into the layers, a charge inversion from positive to negative was observed on the nanohybrid samples. The surfactant DBS anions were located in the interlayer space according to the PXRD pattern of Figure 1b, and once the positive structural charge was balanced, more DBS anions were disposed in a bilayer structure, and a portion of the polar groups was adsorbed on the external surface facing the aqueous solution giving a negative charge to the particles, based on the model proposed by Rojas et al. [39].

2.2. Study of the Am, DGB and BG Removal by MgAlCO3, MgAlNO3 and MgxAlDBS

2.2.1. Adsorption of the Anionic Dyes (Am and DGB)

Am and DGB adsorption tests were carried out with the inorganic LDH (MgAlCO3 and MgAlNO3) and the nanohybrids Mg2AlDBS and Mg3AlDBS for comparison purposes. The influence of pH on the adsorption process could have a relevant role and therefore this one was examined at an initial pH value between 4 and 10 for Am and DGB on MgAlNO3, MgAlCO3, Mg2AlDBS and Mg3AlDBS adsorbents. The final pH was measured after each adsorption experiment, and the maximum value obtained was between 7 and 9.5, which was consistent with the buffering properties of hydrotalcites. The pH influence results included in Table S1 indicated that the maximum adsorption of Am for MgAlCO3 was at pH = 4, probably due to the elimination of the carbonate anion as CO_2 together with some dissolution of the LDH and possibly subsequent recrystallization with Am in the interlayer [40]. However, the adsorption was not significantly affected by the initial pH = 4 and 7 for MgAlNO3 and MgxAlDBS (x = 2 and 3). This led us to adopt an initial pH ~ 6 corresponding to the pH of the Am solutions for all adsorption tests. The DGB adsorption was almost the same at pH 4 and 8, slightly higher at pH 8 for LDH containing inorganic anions, so the pH ~ 8 corresponding to the dye solutions, was used for all the adsorption tests. In general, with the increase of the solution pH, the percentage of the removal of Am and DGB decreases for MgAlCO3 and MgAlNO3 adsorbents due to a decrease in the positive charge on the external surface by deprotonation and competition between the anions (anion dyes and OH^-) for the positive charges of the LDH layer. For nanohybrid samples (MgxAlDBS, x = 2 and 3), the percentage of removal is lower than for the inorganic adsorbents and a decrease in adsorption was observed with the increase of pH solution, due to the repulsion of the negative charges.

The kinetic results of Am and DGB adsorption on the prepared adsorbents are included in Figure 4. The equilibrium for amaranth adsorption on inorganic LDH was reached at 180 min for MgAlCO3 and 360 min for MgAlNO3.

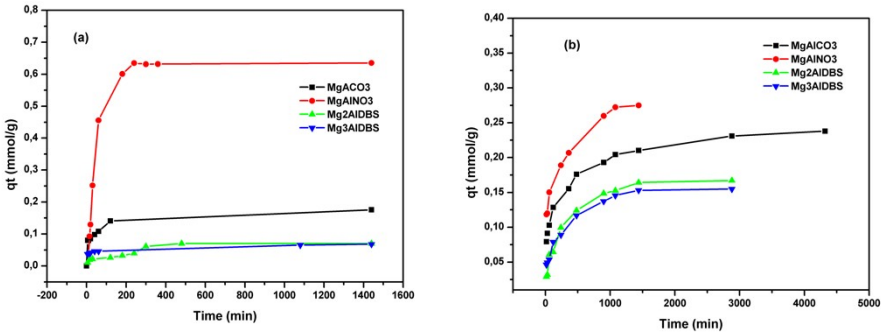

Figure 4. Evolution of dye adsorption on inorganic and nanohybrid LDH for: (**a**) amaranth and (**b**) DGB. qt (mmol/g) is the adsorption capacities of the absorbate at time t (min).

The adsorption of DGB was much slower than that of Am for all adsorbents. The larger size of DGB (29.4 Å × 7 Å for DGB vs. 15 Å × 9 Å for Am, from Chem Draw 3D 5.0 software package Program cause bigger steric hindrances for its adsorption on LDH. Kinetic modelling of the adsorption process provides a prediction of adsorption rates and allows the determination of suitable rate expressions characteristic of possible reaction mechanisms. In this study, the most frequently used models, the pseudo-first-order, Equation (1) [41], the pseudo-second-order, Equation (2) [42], and the intraparticle diffusion model, Equation (3) [43] were tested:

$$\ln(qe - qt) = \ln qe - k_1 t \quad (1)$$

$$\frac{t}{qt} = \frac{1}{k_2 qe^2} + \frac{t}{qe} \quad (2)$$

$$qt = k_{ip} t^{0.5} + C \quad (3)$$

where qe and qt (mmol/g) are the adsorption capacities of the adsorbate at equilibrium and at time t (min), respectively; k_1 (min^{-1}) and k_2 (g $mmol^{-1}$ min^{-1}) are the rate constants of pseudo-first-order and pseudo-second-order models; and k_{ip} (mmol g^{-1} $min^{-1/2}$) is the intraparticle diffusion rate constant. If the intra-particle diffusion is involved in the process, the plot of qt vs. $t^{1/2}$ will be linear, and, if this line passes through the origin, the rate limiting process is only due to the intra-particle diffusion. Such plots may present a multilinearity indicating that two or more steps take place. The slowest of these steps determines the overall rate of the adsorption process [44].

The kinetic parameters calculated for Am and DGB adsorption on the prepared samples are listed in Tables 2 and 3. The pseudo-second-order model is the most suitable in describing the adsorption kinetics of dyes on LDH based on the correlation coefficient (R^2). The applicability of the pseudo-second order suggested that chemisorption might be the rate-limiting step that controls these adsorption processes. Furthermore, the theoretical qe calculated values are closer to the experimental qe values and explain the kinetics of most adsorption systems very well for a whole range of adsorption periods using different concentrations of dye and adsorbent dosages which present an advantage over pseudo-first order equation [45].

Table 2. Kinetic parameters of pseudo-first-order, pseudo-second-order and intra-particle diffusion models for amaranth adsorption by MgAlNO3, MgAlCO3, Mg2AlDBS and Mg3AlDBS.

Adsorbents	qe Exp	Pseudo-1st-Order			Pseudo-2nd-Order			Intra Particle Diffusion		
		k_1	qe	R^2	k_2	qe	R^2	k_{ip}	C	R^2
MgAlNO3	0.64	0.035	0.622	0.985	0.022	0.680	0.999	0.039	−0.012	0.897
MgAlCO3	0.18	0.012	0.157	0.885	0.184	0.184	0.986	0.022	0.086	0.861
Mg2AlDBS	0.07	0.009	0.064	0.733	4×10^{-6}	0.075	0.963	0.018	0.012	0.797
Mg3AlDBS	0.07	0.004	0.028	0.991	0.004	0.068	0.999	0.0008	0.037	0.976

Table 3. Kinetic parameters of pseudo-first-order, pseudo-second-order and intra-particle diffusion models for DGB adsorption by MgAlNO3, MgAlCO3, Mg2AlDBS and Mg3AlDBS.

Adsorbent	qe Exp	Pseudo-1st-Order			Pseudo-2nd-Order			Intra-Particle Diffusion		
		k_1	qe	R^2	k_2	qe	R^2	k_{ip}	C	R^2
MgAlNO3	0.275	0.0001	1.117	0.618	0.058	0.279	0.998	0.003	0.124	0.851
MgAlCO3	0.237	0.007	0.427	0.776	0.030	0.241	0.997	0.002	0.095	0,879
Mg2AlDBS	0.167	0.004	0.138	0.977	0.175	0.037	0.997	0.003	0.035	0.871
Mg3AlDBS	0.155	0.002	0.101	0.939	0.051	0.159	0.997	0.002	0.046	0.891

The adsorption isotherms of the two anionic dyes at room temperature and a constant initial pH of the dye solution are illustrated in Figure 5. The adsorbed amount of the dyes was higher on MgAlNO3 than on MgAlCO3 because of the lower affinity of the nitrate anion for the hydroxide layer favoured the anionic exchange and produced a greater number of adsorption sites. The small amount adsorbed for MgAlCO3 probably occurred over the surface of the adsorbent. The adsorbed amount of both dyes was lower for hybrids than for MgAlNO3, since the external surface charge of the nanohybrid was negative (as suggested by the zeta potential values (Figure S3) and suffers electrostatic repulsion with the sulfonate groups of the dye molecules. The experimental adsorption data were fitted to the Langmuir and Freundlich models, often used to describe adsorption processes and in which lineal forms are represented in Equations (4) and (5), respectively, and the model of Sips, nonlinear form, Equation (6):

$$Ce/qe = (1/qm)Ce + 1/(qmK_L) \quad (4)$$

where qe is the amount of dye adsorbed at equilibrium (mmol·g^{-1}); qm is the maximum monolayer sorption capacity (mmol·g^{-1}); Ce the equilibrium concentration of dye in solution (mmol·L^{-1}) and K_L (L·mmol^{-1}) is a constant related to the sorption energy:

$$\log qe = \log K_f + N_f \log Co \quad (5)$$

where K_f and N_f are the Freundlich constants that are characteristic of the adsorbent–adsorbate systems [46].

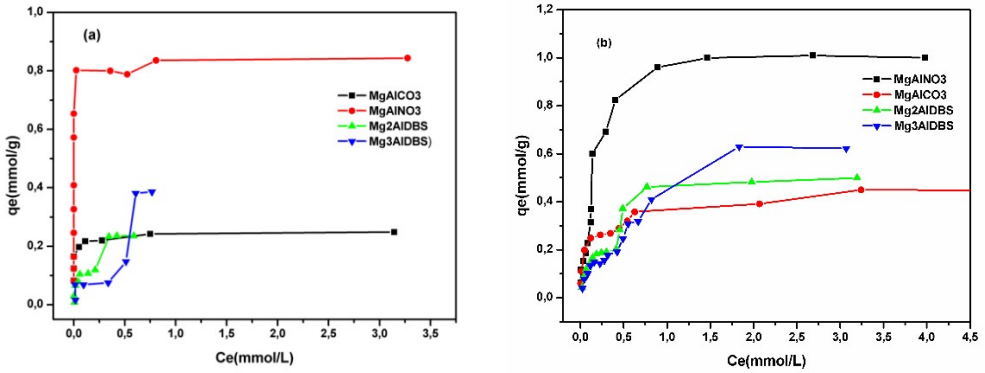

Figure 5. Isotherms data of the dye adsorption (**a**) amaranth and (**b**) DGB by MgAlCO3, MgAlNO3, Mg2AlDBS and Mg3AlDBS adsorbents, qe is the amount of dye adsorbed at equilibrium (mmol·g^{-1}).

The Sips isotherm model [47] is a combination of the Langmuir and Freundlich isotherms that is used to describe heterogeneous adsorption systems:

$$qe = \frac{qmK_sCe^{1/n}}{1 + K_s\,Ce^{1/n}} \quad (6)$$

The Sips isotherm has the advantage of being reduced to the Freundlich isotherm at low concentrations, and at high concentrations approaches the capacity of the formation of a monolayer such as in the case of the Langmuir isotherm. When *n* is equal to 1, the Sips equation is reduced to the Langmuir equation and involves a homogeneous adsorption process.

The influence of the concentration (adsorption isotherms) of Am at room temperature was studied for the four adsorbents and included in Figure 5a. The isotherm shape obtained for MgAlCO3 was of L-type [48] which suggests a progressive saturation of the adsorbent. This type of isotherm is indicative of molecules adsorbed flat on the surface, or sometimes of vertically oriented adsorbed ions with a particularly strong intermolecular attraction. Moreover, the shape of the isotherms was of type H for dye adsorption on MgAlNO3 (Figure 5a,b). The H-curve, whose initial section of the isotherm is vertical, arises in special cases of the L-curve, in which the solute has such a high affinity that it is completely adsorbed in dilute solutions. The adsorbate is strongly attracted to the adsorbent mainly by electrostatic interaction [49].

In solid sorbent adsorption, multilayers often form and there may also be a change of orientation of the adsorbed molecules as they increase in concentration on the adsorbent surface. The adsorption isotherms of both dyes on nanohybrids were of the L-4 subtype, characteristic of the isotherms with two slopes (Figure 5a,b). This isotherm type suggests the possibility of adsorption on different types of sites, successively. In both cases, the shape of the isotherms does not change with the increase in the amount of DBS in the interlayer of the hybrids, indicating that the type of interactions between the hybrids and dyes is not affected by the DBS amount. Tables 4 and 5 include the parameters obtained from fitting the data to the different isotherm models discussed above. It was observed that the isotherms adjusted to the Sips model describe a heterogeneous adsorption, indicated by the R^2 values

obtained. The application of the Freundlich model does not allow a satisfactory refinement of the results in all adsorbents.

Table 4. Parameters of Langmuir, Freundlich and Sips models of Am adsorption by MgAlCO3, MgAlNO3, Mg2AlDBS and Mg3AlDBS.

Adsorbents	Langmuir				Freundlich			Sips			
	qm Exp	qm	K_L	R^2	N_f	K_f	R^2	qm	K_S	n	R^2
MgAlNO3	1.01	1.259	3.06	0.994	0.47	0.897	0,964	1.083	8.2	074	0.998
MgAlCO3	0.44	0.279	60.19	0.978	0.25	0.380	0.938	0.314	14.623	0.71	0.991
Mg2AlDBS	0.50	0.543	3.26	0.982	0.37	0.327	0.998	1.069	0.486	0.49	0.999
Mg3AlDBS	0.63	0.864	0.84	0.998	0.52	0.350	0,.985	0.835	0.9125	1.04	0.999

Table 5. Parameters of Langmuir and Freundlich and Sips models of DGB adsorption by MgAlNO3, MgAlCO3, Mg2AlDBS and Mg3AlDBS.

Adsorbents	Langmuir				Freundlich			Sips			
	qm Exp	qm	K_L	R^2	N_f	K_f	R^2	qm	K_S	n	R^2
MgAlNO3	0.84	0.794	0.0036	0.557	0.318	0.967	0.998	0.789	2431	0.73	0.999
MgAlCO3	0.32	0.221	3083	0.495	0.088	0.251	0.996	0.451	1.218	0.15	0.999
Mg2AlDBS	0.24	0.285	10.30	0.974	0.428	0.315	0.964	0.317	5.549	0.85	0.976
Mg3AlDBS	0.39	0.788	1.368	0.968	0.695	0.492	0.966	0.923	0.998	0.07	0.968

The shape of the adsorption isotherms for the anionic dyes Am and DGB on nanohybrids MgxAlDBS (x = 2 and 3) can be related to the fact that the adsorption at low concentrations occurs through anion exchange mechanism, but, as the concentration of dye increases, the large size of the dyes anions impedes their intercalation and probably occurs on the surface through hydrophobic interactions.

2.2.2. Adsorption of the Cationic Dye BG

The adsorption process for BG was studied on MgAlNO3 and the nanohybrid MgxAlDBS, x = 2 and 3. The results of the adsorption kinetics of the BG cationic dye on the MgAlNO3, Mg2AlDBS and Mg3AlDBS samples shown in Figure 6 indicate that the adsorption equilibrium was reached faster for Mg3AlDBS (in 6 h) and slower for Mg2AlDBS (in 24 h) similar to MgAlNO3.

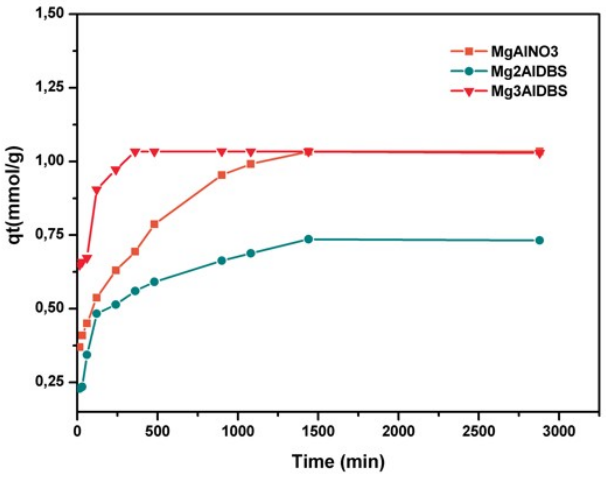

Figure 6. Evolution of BG adsorption on MgAlNO3 and nanohybrids. qt (mmol/g) is the adsorption capacities of the absorbent at time t (min).

The kinetic parameters obtained from the application of the different models are shown in Table 6. The pseudo-second-order model is the most suitable in describing the adsorption kinetics of BG in

all cases, based on the correlation coefficient (R^2) and the agreement between the experimental and calculated values of qe.

Table 6. Kinetic parameters of pseudo-first-order, pseudo-second-order and intra-particle diffusion models for BG adsorption on MgAlNO3, Mg2AlDBS and Mg3AlDBS.

Adsorbants	qe Exp	Pseudo-1st-Order			Pseudo-2nd-Order			Intra Particle Diffusion		
		k_1	qe	R^2	k_2	qe	R^2	k_{ip}	C	R^2
MgAlNO3	1.03	0.008	0.954	0.885	0.008	1.075	0.996	0.015	0.378	0.889
Mg2AlDBS	0.74	2.401	0.998	0.982	0.015	0.752	0.998	0.017	0.292	0.807
Mg3AlDBS	1.03	0.003	0.039	0.228	0.095	1.036	0.999	0.008	0.738	0.563

The results of the adsorption isotherms of the cationic dye BG presented in Figure 7 are of H type [48], suggesting a very high affinity between the adsorbent and the adsorbate.

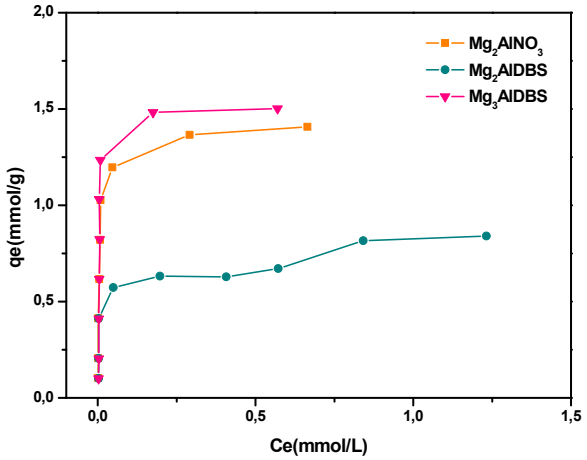

Figure 7. Adsorption isotherms of BG on MgAlNO3 and the nanohybrids, qe is the amount of dye adsorbed at equilibrium (mmol·g^{-1}).

According to the results shown in Table 7, for the three adsorbents, the Sips model fits the experimental data of adsorption equilibrium better than the other models and this is used to describe heterogeneous adsorption systems. The *n* value is near to 1 for MgAlNO3, therefore adsorption can be represented more appropriately by a monolayer adsorption. However, the nanohybrids MgxAlDBS (x = 2 and 3) show a value of *n* much lower than 1; therefore, the adsorption is not represented by a homogeneous process.

Table 7. Parameters of Langmuir, Freundlich and Sips isothermal models of BG adsorption by MgAlNO3, Mg2AlDBS and Mg3AlDB.

Adsorbents	Langmuir				Freundlich			Sips			
	qm Exp	qm	K_L	R^2	N_f	K_f	R^2	qm	Ks	n	R^2
MgAlNO3	1.40	1.40	190	0.968	0.17	1.62	0.817	1.373	425.2	0.87	0.971
Mg2AlDBS	0.84	154.50	0.82	0.850	0.17	0.87	0.786	1.622	1.1	0.69	0.862
Mg3AlDBS	1.50	1.53	155	0.977	0.18	1.80	0.873	1.492	38485	0.50	0.999

The high amount of BG adsorbed on inorganic LDH could be due to the hydrotalcite buffer properties, i.e., initial pH solution increases during experiments, which provokes the precipitation of this dye. Nevertheless, for MgxAlDBS (x = 2 and 3) adsorbents, DBS incorporation changes the electrical properties of the particles making the surface potential negative (according to the zeta

potential shown in Figure S3) and favours the adsorption of cationic dye. Surprisingly, a minor amount of BG was adsorbed on the Mg2AlDBS regarding the Mg3AlDBS sample, which has a higher permanent charge due to the isomorphic substitution of divalent for trivalent metal, and, consequently, a higher DBS content. It could be because the higher DBS loading on Mg2AlDBS provokes steric hindrances for BG intercalation and, in the case of Mg3AlDBS, there is probably some cationic dye co-intercalated with DBS in the interlayer space as will be suggested below by the PXRD pattern of adsorption product (Figure S6c).

2.2.3. Characterization of the Adsorption Products

The solids obtained after the adsorption experiments were analyzed by the PXRD technique in order to ascertain how the dye is located in the adsorbent. Figures S4 and S5 show the PXRD patterns of the products of Am and DGB adsorption, respectively, together with the patterns of the adsorbents and of the dyes. The results indicated that the positions of the diffraction lines of the MgAlCO3 sample were not modified after the Am and DGB adsorption process, possibly due to the fact that the small amounts of dye were adsorbed on the external surface of the adsorbent. However, for the Am adsorption product obtained with MgAlNO3, the PXRD pattern included in Figure S4a shows a shift in the position of the reflection lines (*00l*) to the lower angle (2θ) with a change in the $d_{(003)}$ value from 8.9 Å to 17.7 Å. These lines were very sharp, indicating that the adsorption product retained the crystallinity of the adsorbent according to an anionic exchange process [49]. Similar results were obtained for the DGB adsorption product. However, in this case, the DGB intercalation process is strongly dependent on the concentration of the dye. The PXRD pattern included in Figure S5a shows a shift of the position of reflection line corresponding to $d_{(003)}$ = 8.9 Å to 15.3 Å at low DGB concentration (0.06 mmol/L) according to the intercalation of the anion in the interlayer space. However, at a high DGB concentration (3.7 mmol/L), the interlayer space does not increase any further, indicating that the adsorption takes place on the external surface of the particles, which can be attributed to the large size and elongated shape of the dye anion. The adsorption of dye occurs provided the interlayer spacing of the LDH is greater than the size of the molecule; otherwise, the adsorbent can not accommodate the pollutant [1]. At low concentrations of dye, it is possible to intercalate the DGB ions in a parallel manner or with a small inclination with respects to the sheets of LDH, giving rise to an interlayer space close to that observed in Figure S5a (15.3 Å). This disposition of the ions would allow the cancellation of the layer charge by means of the electrostatic interaction with the sulfonate groups. However, as the concentration of the dye increases, the arrangement of bulky ions becomes more difficult, thus impeding their intercalation and favouring the adsorption on the external surface of the LDH particles.

The PXRD patterns of the Am adsorption products on nanohybrids adsorbents (Figure S4c,d) showed no change in the position of the planes (*00l*), so it can be deduced that the adsorption takes place on the external surface of the particles in the adsorbents studied. Similar results were obtained for the DGB adsorption products on nanohybrids (Figure S5b).

The PXRD patterns of the BG adsorption products are shown in Figure S6. It is interesting to note that there are no changes between the adsorbent Mg2AlDBS and the adsorption product Mg2 AlDBS-BG Figure S6a,b. However, in the case of Mg3AlDBS, a decrease in the basal spacing of the adsorption product Mg3AlDS-BG compared with the pristine adsorbent, from d_{003} = 30 Å to d_{003} = 27.3 Å Figure S6c, is observed. The reason for this decrease could be the change of orientation of the DBS chains as a result of some co-intercalation of BG between them [50,51].

Table 8 shows the maximum adsorption capacity of some adsorbents compared to the double layered hydroxides prepared in this study. It was observed that the LDH reach the highest adsorption values due to their structural characteristics, anion exchange capacity, the intercalation of anion and/or the ability to modify the hydrophilic nature of the interlaminar space.

Table 8. Maximum adsorption capacity of several adsorbents used to remove the dyes Am, DGB and BG.

Adsorbent	Dye	qm (mmol/g)	Reference
MgAlNO3	Am	0.8	This study
MgAlCO3	Am	0.2	This study
Mg2AlDBS	Am	0.29	This study
Mg3AlDBS	Am	0.466	This study
FeO_3ZnO_2/Rgo	Am	0.13	[52]
Ashes	Am	0.013	[53]
Alumina/polystyrene	Am	0.033	[54]
MgAlNO3	DGB	1.089	This study
MgAlCO3	DGB	0.305	This study
Mg2AlDBS	DGB	0.557	This study
Mg3AlDBS	DGB	0.791	This study
Mahogany sawdust	DGB	0.4	[55]
Polyaniline	DGB	0.26	[56]
AC/CP	DGB	0.15	[57]
MgAlNO3	BG	1.418	This study
Mg2AlDBS	BG	0.827	This study
Mg3AlDBS	BG	1.534	This study
Ni-SBA-16	BG	0.66	[58]
Red clay	BG	0.26	[59]

3. Materials and Methods

The inorganic salts were supplied by Panreac (Barcelona, Spain). The organic salts used for the preparation of the organo-LDH nanohybrids containing DBS and the dyes, were supplied by Sigma-Aldrich (Barcelona, Spain). The dyes used were: Amaranth (Am) (trisodium 3-oxo-4-[(4-sulfonatonaphthalen-1-yl)hydrazinylidene] naphthalene-2,7-disulfonate) whose empirical formula is $C_{20}H_{11}N_2Na_3O_{10}S_3$ and the formula mass is 604.47. This dye presents a maximum absorption at λ = 520 nm. Diamine green B (DGB) (disodium 4-amino-5-hydroxy-3-[[4′-[(4-hydroxyphenyl)azo] [1,1′-biphenyl]-4-yl]azo]-6-(phenylazo)naphthalene-2,7-disulphonate whose empirical formula is $C_{34}H_{22}N_8Na_2O_{10}S_2$ and the formula mass is 812.7, presents a maximum absorption at λ = 623 nm. Brilliant green (BG) (4-(4-(diethylamino)-alpha-phenylbenzylidene)-2,5-cyclohexadien-1-ylidene) diethylammonium sulfate whose empirical formula is $C_{27}H_{34}N_2O_4S$ and the formula mass is 482.63, presents a maximum absorption at λ = 624 nm.

The estimated bidimensional molecular size of the dyes was calculates from ChemDraw 3D 5.0 software package program and it has been included in Figure 8.

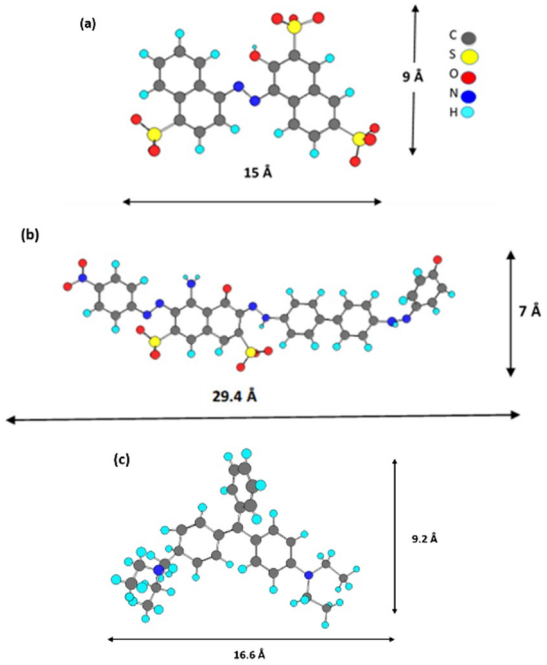

Figure 8. Chemical structure of the dyes: (**a**) Amaranth, (**b**) Diamine green B and (**c**) Brilliant green.

3.1. Synthesis of the Adsorbents

3.1.1. Synthesis of MgAlCO3 and MgAlNO3 Samples

$MgAlCO_3$ was coprecipitated by the drop wise addition of a $Mg(NO_3)_2{\cdot}6H_2O$ and Al $(NO_3)_3{\cdot}9H_2O$ mixed aqueous solution of 1 M concentration of metal in 100 mL, with Mg/Al ratio = 2, to a solution of 2 M Na_2CO_3; 2 M NaOH aqueous solution was simultaneously added to keep the pH constant at 10.0 ± 0.3. The MgAlNO3 sample was also co-precipitated using the same concentration of metal aqueous solution, but this was added to 100 mL of distilled and CO_2-free water by passing N_2 current. The reaction was carried out under N_2 to minimize carbonate contamination from atmospheric CO_2 and 2 M NaOH aqueous solution was simultaneously added to keep the pH constant at 10.0 ± 0.3. In both cases, the resulting suspensions were hydrothermally treated at 80 °C and then washed and dried at 60 °C [21].

3.1.2. Synthesis of MgxAlDBS (x = 2 and 3) Samples

The nanohybrids, LDH containing DBS anions with Mg/Al = 2 and 3 ratios, were obtained by the coprecipitation method using N_2 atmosphere and CO_2-free water. For the Mg2AlDBS sample, a solution A containing a mixture of 0.04 mol of $Mg(NO_3)_2{\cdot}6H_2O$ and 0.02 mol of $Al(NO_3)_3{\cdot}9H_2O$ in 100 mL of distilled and CO_2-free water, was added drop wise to a solution B containing 0.12 mol of NaOH and 0.05 mol of dodecylbenzene sulfonate in 500 mL. The resulting suspension was hydrothermally treated at 80 °C and then washed and dried at 60 °C. The procedure for the synthesis of the Mg3AlDBS sample was the same, except that the solution A contained a mixture of 0.06 mol of $Mg(NO_3)_2{\cdot}6H_2O$ and 0.02 mol of $Al(NO_3){\cdot}9H_2O$ in 100 mL of distilled and CO_2-free water [26].

3.2. Adsorption Experiments

Dye adsorption isotherms on the prepared adsorbents were obtained by the batch equilibration procedure. Duplicate 25 mg adsorbent samples were equilibrated by shaking at room temperature with 25 mL of dye solutions with initial concentrations (Co) ranging between 0.083 $mmol{\cdot}L^{-1}$ and 6.62 $mmol{\cdot}L^{-1}$ for Am, 0.061 $mmol{\cdot}L^{-1}$ and 3.69 $mmol{\cdot}L^{-1}$ for DGB and 0.10 $mmol{\cdot}L^{-1}$ and 2.02 $mmol{\cdot}L^{-1}$ for BG $mmol{\cdot}L^{-1}$. After a suitable contact time of equilibration, the supernatants were

centrifuged and separated to determine the concentration of the dyes by UV-visible Spectrophotometry. The amount of dye adsorbed (qe) was calculated from the difference between the initial (Co) and equilibrium (Ce) solution concentrations.

3.3. Experimental Techniques

Elemental chemical analyses were obtained using ICP-mass spectrometry after the dissolution of the solids in 0.1 M HCl (PerkinElmer Nexion X), XRD patterns of powdered samples were recorded on a Bruker D8 discover 28 instrument, the measurements were carried out at room temperature under atmospheric conditions, Cu Kα radiation (λ = 1.5405 Å) was used, and the step size and step counting time used were 0.02°(2θ) and 0.65 s, respectively. FT-IR spectra were obtained on a PerkinElmer Spectrum Two spectrophotometer by using a KBr disk method (the disk containing approximately 1 wt.% of sample in KBr). Nitrogen adsorption–desorption isotherms were recorded on a Micromeritics ASAP 2101 apparatus), using samples previously outgassed at 100 °C under vacuum for 1 h. Specific surface areas (SSA) were calculated by applying the BET method over the relative equilibrium pressure range $0.05 < P/P_0 < 0.30$, in the N_2 adsorption isotherms. Scanning electron microscopy (SEM) micrographs were obtained using a JEOL JSM 6300 instrument; the samples were prepared by deposition of a drop of sample suspension on a Cu sample holder and covered with an Au layer by sputtering in a Baltec SCD005 apparatus). Thermogravimetric analysis (TGA) was carried out in NETZSCH Leading equipment at a heating rate of 5 °C·min^{-1} in nitrogen atmosphere. Zeta potential measurements were carried out on Zetasizer Nano ZSP Malvern.

4. Conclusions

We examined four samples as potential adsorbents of amaranth (Am), diamine green B (DGB) and brilliant green (BG) dyes from simulated wastewaters. The prepared products are two layered doubled hydroxides (LDH) with carbonate and nitrate as interlayer anion (MgAlCO3 and MgAlNO3) and two nanohybrids of LDH intercalated with dodecylbenzene sulfonate (MgxAlDBS, x = 2 and 3).

The key findings of this study are:

- According to the kinetic studies, the adsorption equilibrium of the dyes was reached in 3 h with LDH containing inorganic anions and less than 24 h for the nanohybrids LDH.
- The dye adsorption process follows the pseudo-second order model in all cases, although it is slower for the cationic dye (BG) than for the anionic ones (Am and DGB), which could be due to its bulky size.
- The three dyes have a high affinity for MgAlNO3. The structural analysis (PRXD) of the adsorption products suggests that the adsorption at low concentrations occurs through anion exchange. However, at high dye concentrations, the adsorption probably occurs on the LDH surface through hydrophobic interactions. This could be because the large size of the dye anions hinders their intercalation. The adsorption isotherms of Am and DGB adsorption on the MgxAlDBS (x = 2 and 3) samples occurs in two steps, which suggests the possibility of adsorption on different types of sites.
- According to the PXRD patterns of the adsorption products, the BG adsorption takes place on the external surface of the particles in the three adsorbents studied. This adsorption works best in the nanohybrid samples, probably due to the precipitation of the dye together with the co-intercalation process and/or multilayer adsorption over the DBS (interlayer anion).
- Different types of interactions, such as electrostatic interactions, ion exchange, hydrogen bonding and van der Waals forces, may be involved in the adsorption process, whose interaction dominating the process depends on the nature of the adsorbent and adsorbate.
- The optimal conditions for the adsorption of Am and DGB were for the unmodified pH of the dye solution. The maxima adsorption was achieved for the MgAlNO3 sample.

As such, we found that MgAlNO3 and nanohybrids MgxAlDBS may be used in the design of adsorbents for the removal of anionic and cationic dyes to reduce their adverse effect on water resources.

Supplementary Materials: The following are available online at http://www.mdpi.com/2305-7084/3/2/41/s1, Figure S1: TG curves in N_2 atmosphere of the samples (a) Mg2AlDBS and (b) Mg3AlDBs Figure 2: Adsorption–desorption isotherms of N_2 on the LDHs samples (a) MgAlNO3 and MgAlCO3 and (b) Mg2AlDBS and Mg3AlDBS. Figure S3: Zeta potential values obtained in a KCl solution (0.01 M) at pH between 2 and 12 of the adsorbents: MgAlNO3, MgAlCO3, Mg2AlDBS and Mg3AlDBS. Figure S4: PXRD patterns of the Am adsorption products on the LDH samples: (a) MgAlNO3, (b) MgAlCO3, (c) Mg2AlDBS and (c) Mg3AlDBS. Figure S5: PXRD patterns of the DGB adsorption products on the LDH samples: (a) MgAlNO3, and (b) Mg3AlDBS. Figure S6: PXRD patterns of the BG adsorption products on the LDH samples: (a) MgAlNO3, (b) Mg2AlDBS and (c) Mg3AlDBS. Table S1: Values of the initial and final pH of the adsorption process and the percentage of Am and DGB dyes adsorbed by MgAlCO3, MgAlNO3, Mg2AlDBS and Mg3AlDBS. Co = 0.16 mmol·L^{-1} except for the Am adsorption experiment by MgAlNO3 Co = 1.7 mmol·L^{-1}, solid solution ratio = 1 g/L.

Author Contributions: Conceptualization, I.P. and C.B.; methodology, I.P. and C.B.; investigation, K.A.; writing—original draft preparation, I.P. and C.B.; writing—review and editing, I.P. and C.B.; supervision, C.B.

Funding: This work was funded by the Spanish Junta de Andalucía (Research Group FQM-214).

Acknowledgments: K.A. thanks the PNE program scholarships from Ministere de L'Enseignement Superieur et de la Recherche Scientifique. The authors appreciate the technical assistance received in the SCAI (Universidad de Córdoba) for Elemental Analysis (ICP-MS) and Electron Microscopy Units.

Conflicts of Interest: The authors declare no conflict of interest.

References

1. Forano, C. Environmental remediation involving layered double hydroxides. In *Clay Surfaces—Fundamentals and Applications*; Wypych, F., Satyanarayana, K.G., Eds.; Elsevier Academic Press: Cambridge, MA, USA, 2004; pp. 425–458.
2. Rojas, R. Applications of Layered Double Hydroxides on environmental remediation. In *Hydroxides: Synthesis, Types and Applications*; Carrillo, A.C., Griego, D.A., Eds.; Nova Science Publishers: New York, NY, USA, 2012; pp. 39–71.
3. Mall, I.D.; Srivastava, V.C.; Agarwal, N.K. Removal of Orange-G and Methyl Violet dyes by adsorption onto bagasse fly ash-kinetic study and equilibrium isotherm analyses. *Dyes Pigments* **2006**, *69*, 210–223. [CrossRef]
4. Wong, Y.; Szeto, Y.; Cheung, W.; McKay, G. Adsorption of acid dyes on chitosan–Equilibrium isotherm analyses. *Process Biochem.* **2004**, *39*, 693–702. [CrossRef]
5. Al-Degs, Y.S.; El-Barghouthi, M.I.; El-Sheikh, A.H.; Walker, G.A. Effect of solution pH, ionic strength, and temperature on adsorption behavior of reactive dyes on activated carbon. *Dyes Pigments* **2008**, *77*, 16–23. [CrossRef]
6. Rafatullah, M.; Sulaiman, O.; Hashim, R.; Ahmad, A. Adsorption of methylene blue on low-cost adsorbents: A review. *J. Hazard. Mater.* **2010**, *177*, 70–80. [CrossRef] [PubMed]
7. Batzias, F.A.; Sidiras, D.K. Dye adsorption by prehydrolysed beech sawdust in batch and fixed-bed systems. *Bioresour. Technol.* **2007**, *98*, 1208–1217. [CrossRef]
8. Otero, M.; Rozada, F.; Calyo, L.F.; Garcia, A.I.; Moran, A. Elimination of organic water pollutants using adsorbents obtained from sewage sludge. *Dyes Pigments* **2003**, *57*, 55–65. [CrossRef]
9. Malik, P.K. Use of activated carbons prepared from sawdust and rice-husk for adsorption of acid dyes: A case study of Acid Yellow 36. *Dyes Pigments* **2003**, *56*, 239–249. [CrossRef]
10. Singh, D.K.; Srivastaya, B. Basic dyes removal from wastewater by adsorption on rice husk carbon. *Indian J. Chem. Technol.* **2001**, *8*, 133–139.
11. Lee, S.H.; Song, D.I.; Jeon, Y.W. An investigation of the adsorption of organic dyes onto organo-montmorillonite. *Environ. Technol.* **2001**, *22*, 247–254. [CrossRef] [PubMed]
12. Crini, G. Non-conventional low-cost adsorbents for dye removal: A review. *Bioresour. Technol.* **2006**, *97*, 1061–1085. [CrossRef]
13. Mahmoodi, N.M.; Salehi, R.; Arami, M.; Bahrami, H. Dye removal from colored textile wastewater using chitosan in binary system. *Desalination* **2011**, *267*, 64–72. [CrossRef]
14. Gupta, V.K.; Suhas. Application of low-cost adsorbents for dye removal—A review. *J. Environ. Manag.* **2009**, *90*, 2313–2342. [CrossRef] [PubMed]
15. Wu, P.; Wu, T.; He, W.; Sun, L.; Li, Y.; Sun, D. Adsorption properties of dodecylsulfate-intercalated layered double hydroxide for various dyes in water. *Colloid Surf. A Physicochem. Eng. Asp.* **2013**, *436*, 726–731. [CrossRef]

16. Extremera, R.; Pavlovic, I.; Pérez, M.R.; Barriga, C. Removal of acid orange 10 by calcined Mg/Al layered double hydroxides from water and recovery of the adsorbed dye. *Chem. Eng. J.* **2012**, *213*, 392–400. [CrossRef]
17. Bruna, F.; Pavlovic, I.; Celis, R.; Barriga, C.; Cornejo, J.; Ulibarri, M.A. Organohydrotalcites as novel supports for the slow release of the herbicide terbuthylazine. *Appl. Clay Sci.* **2008**, *42*, 194–200. [CrossRef]
18. Rives, V. *Layered Double Hydroxides: Present and Future*; Nova Science Publishers, Inc.: New York, NY, USA, 2001.
19. Abdellaoui, K.; Pavlovic, I.; Bouhent, M.; Benhamou, A.; Barriga, C. A comparative study of the amaranth azo dye adsorption/desorption from aqueous solutions by layered double hydroxides. *Appl. Clay Sci.* **2017**, *143*, 142–150. [CrossRef]
20. Shan, R.; Yan, L.; Yang, Y.; Yang, K.; Yu, S.; Yu, H.; Zhu, B.; Du, B. Highly efficient removal of three red dyes by adsorption onto Mg–Al-layered double hydroxide. *J. Ind. Eng. Chem.* **2015**, *21*, 561–568. [CrossRef]
21. Meyn, M.; Beneke, K. Anion-exchange reactions of layered double hydroxides. *Inorg. Chem.* **1990**, *29*, 5201–5207. [CrossRef]
22. Clearfield, A.; Kieke, M.; Kwan, J.; Colon, J.; Wang, R.C. Intercalation of dodecylsulfate into layered double hydroxides. *J. Incl. Phenom. Mol. Recognit. Chem.* **1991**, *11*, 361–378. [CrossRef]
23. Wang, C.; Juang, L.; Lee, C.; Hsu, T.; Lee, J.; Chao, H. Effects of exchanged surfactant cations on the pore structure and adsorption characteristics of montmorillonite. *J. Colloid Interface Sci.* **2004**, *280*, 27–35. [CrossRef]
24. Costa, F.R.; Leuteritz, A.; Wagenknecht, U.; Jehnichen, D.; Haeussler, L.; Heinrich, G. Intercalation of Mg–Al layered double hydroxide by anionic surfactants: Preparation and characterization. *Appl. Clay Sci.* **2008**, *38*, 153–164. [CrossRef]
25. Celis, R.; Koskinen, W.; Hermosin, M.; Ulibarri, M.; Cornejo, J. Triadimefon interactions with organoclays and organohydrotalcites. *Soil Sci. Soc. Am. J.* **2000**, *64*, 36–43. [CrossRef]
26. Bruna, F.; Pavlovic, I.; Barriga, C.; Cornejo, J.; Ulibarri, M.A. Adsorption of pesticides Carbetamide and Metamitron on organohydrotalcite. *Appl. Clay Sci.* **2006**, *33*, 116–124. [CrossRef]
27. Zhou, Q.; Xi, Y.; He, H.; Frost, R.L. Application of near infrared spectroscopy for the determination of adsorbed p-nitrophenol on HDTMA organoclay-implications for the removal of organic pollutants from water. *Spectrochim. Acta Part A Mol. Biomol. Spectrosc.* **2008**, *69*, 835–841. [CrossRef]
28. Laha, S.; Tansel, B.; Ussawarujikulchai, A. Surfactant-soil interactions during surfactant-amended remediation of contaminated soils by hydrophobic organic compounds: A review. *J. Environ. Manag.* **2009**, *90*, 95–100. [CrossRef] [PubMed]
29. Bruna, F.; Celis, R.; Pavlovic, I.; Barriga, C. Layered double hydroxides as adsorbents and carriers of the herbicide (4-chloro-2-methylphenoxy) acetic acid (MCPA): Systems Mg–Al, Mg–Fe and Mg–Al–Fe. *J. Hazard. Mater.* **2009**, *168*, 1476–1481. [CrossRef]
30. Singh, K.; Arora, S. Removal of Synthetic Textile Dyes From Wastewaters: A Critical Review on Present Treatment Technologies. *Crit. Rev. Environ. Sci. Technol.* **2011**, *41*, 807–878. [CrossRef]
31. Braterman, P.S.; Xu, Z.P.; Yarberry, F. Layered double hydroxides (LDHs). In *Handbook of Layered Materials*; Auerbach, S.M., Carrado, K.A., Dutta, P.K., Eds.; Marcel Dekker, Inc.: New York, NY, USA, 2004; pp. 373–474.
32. You, Y.; Zhao, H.; Vance, G.F. Surfactant-enhanced adsorption of organic compounds by layered double hydroxides. *Colloids Surf. A* **2002**, *205*, 161–172. [CrossRef]
33. Ulibarri, M.A.; Pavlovic, I.; Barriga, C.; Hermosín, M.C. Adsorption of anionic species on hydrotalcite-like compounds: Effect of interlayer anion and crystallinity. *Appl. Clay Sci.* **2001**, *33*, 116–124. [CrossRef]
34. Crepaldi, E.L.; Pavan, P.C.; Valim, J.B. Comparative study of the coprecipitation methods for the preparation of layered double hydroxides. *J. Braz. Chem. Soc.* **2000**, *11*, 64–70. [CrossRef]
35. Zhao, H.; Nagy, K.L. Dodecyl sulfate–Hydrotalcite nanocomposites for trapping chlorinated organic pollutants in water. *J. Colloid Interface Sci.* **2004**, *274*, 613–624. [CrossRef] [PubMed]
36. Pavan, P.; Crepaldi, E.; Gomes, G.; Valim, J. Adsorption of sodium dodecylsulfate on a hydrotalcite-like compound. Effect of temperature, pH and ionic strength. *Colloids Surf. A* **1999**, *154*, 399–410. [CrossRef]
37. Sing, K.S. Reporting physisorption data for gas/solid systems with special reference to the determination of surface area and porosity (Recommendations 1984). *Pure Appl. Chem.* **1985**, *57*, 603–619. [CrossRef]
38. Forano, C.; Hibino, T.; Leroux, F.; Taviot-Guého, C. Layered Double Hydroxides. *Dev. Clay Sci.* **2006**, *1*, 1021–1095.

39. Rojas, R.; Bruna, F.; de Pauli, C.P.; Ulibarri, M.A.; Giacomelli, C.E. The effect of interlayer anion on the reactivity of Mg-Al layered double hydroxides: Improving and extending the customization capacity of anionic clays. *J. Colloid Interface Sci.* **2011**, *356*, 136–141. [CrossRef] [PubMed]
40. Hermosín, M.C.; Pavlovic, I.; Ulibarri, M.; Cornejo, J. Hydrotalcite as sorbent for trinitrophenol sorption capacity and mechanism. *Water Res.* **1996**, *30*, 171–177. [CrossRef]
41. Lagergren, S.; Sven, K. About the theory of so-called adsorption of soluble substances. *Sven. Vetensk. Handl.* **1898**, *24*, 1–39.
42. McKay, G. The Adsorption of basic dye onto silica from aqueous solution—Solid diffusion model. *Chem. Eng. Sci.* **1984**, *39*, 129–138. [CrossRef]
43. Weber, W.; Morris, J. Kinetics of adsorption on carbon from solution. *J. Sanit. Eng. Div. Am. Soc. Civ. Eng.* **1963**, *89*, 31–59.
44. Crini, G.; Badot, P.M. Application of chitosan, a natural aminopolysaccharide, for dye removal from aqueous solutions by adsorption processes using batch studies: A review of recent literature. *Prog. Polym. Sci.* **2008**, *33*, 399–447. [CrossRef]
45. Ho, Y.S.; Mckay, G. Sorption of dye from aqueous solution by peat. *Chem. Eng. J.* **1999**, *70*, 115–124. [CrossRef]
46. Travis, C.C.; Etnier, E.L. A survey of sorption relationships for reactive solutes in soil. *J. Environ. Qual.* **1981**, *10*, 8–17. [CrossRef]
47. Sips, R. On the Structure of a Catalyst Surface. *J. Chem. Phys.* **1948**, *16*, 490–495. [CrossRef]
48. Giles, C.H.; MacEwan, T.H.; Nakhwa, S.N.; Smith, D. Studies in Adsorption: Part XI. A System of Classification of Solution Adsorption Isotherms and Its Use in Diagnosis of Adsorption Mechanisms and in Measurement of Specific Surface Area Solids. *J. Chem. Soc.* **1960**, *14*, 3973–3993. [CrossRef]
49. Chaara, D.; Pavlovic, I.; Bruna, F.; Ulibarri, M.A.; Draoui, K.; Barriga, C. Removal of nitrophenol pesticides from aqueous solutions by layered double hydroxides and their calcined products. *Appl. Clay Sci.* **2010**, *50*, 292–298. [CrossRef]
50. Milanesio, M.; Conterosito, E.; Viterbo, D.; Perioli, L. New Efficient Intercalation of Bioactive Molecules into Layered Double Hydroxide Materials by Solid-State Exchange: An in Situ PXRD Study. *Cryst. Growth Des.* **2010**, *10*, 4710–4712. [CrossRef]
51. Conterosito, E.; van Beek, W.; Palin, L. Development of a fast and clean intercalation method for organic molecules into layered double hydroxides. *Cryst. Growth Des.* **2013**, *13*, 1162–1169. [CrossRef]
52. Jiang, H.; Chen, P.; Zhang, W.; Luo, S.; Luo, X.; Au, C.; Li, M. Deposition of nano Fe_3O_4@ZrO_2 onto exfoliated graphite oxide sheets and its application for removal of amaranth. *Appl. Surf. Sci.* **2014**, *317*, 1080–1089. [CrossRef]
53. Mittal, A.; Kurup, L.; Gupta, V.K. Use of waste materials—Bottom ash and de-oiled soya, as potential adsorbents for the removal of amaranth from aqueous solutions. *J. Hazard. Mater.* **2005**, *117*, 171–178. [CrossRef] [PubMed]
54. Ahmad, R.; Kumar, R. Adsorption of amaranth dye onto alumina reinforced polystyrene. *Clean Soil Air Water* **2011**, *39*, 74–82. [CrossRef]
55. Malik, P.K. Dye removal from wastewater using activated carbon developed from sawdust: Adsorption equilibrium and kinetics. *J. Hazard. Mater.* **2004**, *113*, 81–88. [CrossRef] [PubMed]
56. Geetha, K.; Velmani, N.; Karthikeyan, S.; Shabudeen, S. Comparison on equilibrium and kinetic studies on the removal of direct green 6 from aqueous solutions using activated carbons prepared from agro waste. *Dig. J. Nanomater. Biostruct.* **2016**, *11*, 199–212.
57. Geetha, A.; Palanisamy, P.N. Kinetics and Equilibrium Studies on The Removal of Anionic Dyes using Polyaniline Coated Sawdust Composite. *Int. J. Chem. Techol. Res.* **2015**, *7*, 2439–2447.
58. Shah, A.T.; Din, M.I.; Kanwal, F.N.; Mirza, M.L. Direct synthesis of mesoporous molecular sieves of Ni-SBA-16 by internal pH adjustment method and its performance for adsorption of toxic Brilliant Green dye. *Arab. J. Chem.* **2015**, *8*, 579–586. [CrossRef]
59. Rehman, M.S.U.; Munir, M.; Ashfaq, M.; Rashid, N.; Nazar, M.F.; Danish, M.; Han, J.I. Adsorption of Brilliant Green dye from aqueous solution onto red clay. *Clay Chem. Eng. J.* **2013**, *228*, 54–62. [CrossRef]